Study of Injection Molded Microcellular Polyamide-6 Nanocomposites

MINGJUN YUAN[1], LIH-SHENG TURNG[1]*, SHAOQIN GONG[1], DANIEL CAULFIELD[2], CHRIS HUNT[2], *and* RICK SPINDLER[3]

[1]*Polymer Engineering Center*
Department of Mechanical Engineering
University of Wisconsin-Madison
Madison, WI 53706

[2]*USDA Forest Products Laboratory*
Madison, WI 53726

[3]*Kaysun Corporation*
Manitowoc, WI 54221

This study aims to explore the processing benefits and property improvements of combining nanocomposites with microcellular injection molding. The microcellular nanocomposite processing was performed on an injection-molding machine equipped with a commercially available supercritical fluid (SCF) system. The molded samples produced based on the Design of Experiments (DOE) matrices were subjected to tensile testing, impact testing, Dynamic Mechanical Analysis (DMA), and Scanning Electron Microscope (SEM) analyses. Molding conditions and nano-clays have been found to have profound effects on the cell structures and mechanical properties of polyamide-6 (PA-6) base resin and nanocomposite samples. The results show that microcellular nanocomposite samples exhibit smaller cell size and uniform cell distribution as well as higher tensile strength compared to the corresponding base PA-6 microcellular samples. Among the molding parameters studied, shot size has the most significant effect on cell size, cell density, and tensile strength. Fractographic study reveals evidence of different modes of failure and different regions of fractured structure depending on the molding conditions. Polym. Eng. Sci. 44:673–686, 2004.

INTRODUCTION

Polyamide-6 (PA-6) has been widely used in electronics, consumer products, and engineering parts. PA-6/clay nanocomposite also represents a new type of high-performance material, in which platelets of montmorillonite (MMT) clay, about 1 nm in thickness and over 100 nm in lateral dimension, are dispersed in polymer matrices. Owing to the large surface-to-volume ratio of the nano-clay, it offers improved stiffness, heat resistance, barrier and flame retardation, and dimensional stability with a small clay load (< 10%) (1–6). The market potential for nanocomposites is enormous. Extensive work has been carried out in research laboratories and industrial production sites. However, commercialization and industrial applications of nanocomposites have been slow, partially because of the relatively high material cost compared to conventional polymeric materials.

On the other hand, polymeric foams have been widely used because of their beneficial properties such as light weight, thermal and acoustic insulation, and improved energy-absorption performance on impact. Microcellular foam, which is characterized by cell size in the range of 1 to 100 microns, provides further improved mechanical and thermal properties such as high strength/weight ratio, and enhanced toughness and fatigue life of parts (7–11). Even though a recent report shows that microcellular structure may not universally increase impact strength (12), the advantages of microcellular structures have attracted significant attention from the polymer community, which has led to the development of various microcellular foaming techniques applied to such processes as batch foaming

*To whom correspondence should be addressed.

Published online in Wiley InterScience (www.interscience.wiley.com).
DOI 10.1002/pen.20061

(13–16), thermoforming (17), continuous filament and sheet extrusion (18–21), and injection molding (22–25). Among them, the microcellular injection molding process is one of the most promising methods and was first commercialized by Trexel (25).

In microcellular injection molding, "supercritical" nitrogen (N_2) or carbon dioxide (CO_2) is injected into the machine barrel and dissolved into polymer melt to create a single-phase polymer-gas solution. It is capable of producing parts with a microcellular structure while using lower injection pressure, shorter cycle time, and less material. It eliminates the need for a packing stage and improves the dimensional stability of the molded parts. Microcells also greatly enhance the part toughness of many polymeric materials by acting as crack arrestors. For nanocomposites, microcellular injection molding has the potential to produce a component that has excellent physical and mechanical properties at a significantly reduced part weight and material cost.

Substantial research and development have been conducted on the processing and characterization of many different microcellular and filled plastics (26–30). However, the foaming process and cell structure of PA-6 in microcellular processing are very difficult to control because of the high crystallinity and different thermomechanical histories of materials. Recent studies have shown that the addition of the nano-clay fillers greatly increases the viscosity of the polymer (31). On the other hand, blending supercritical gas into a polymer melt effectively reduces the viscosity and the glass transition temperature of the polymer melt, as well as the interfacial tension (32). Hence, adding supercritical gas into nanocomposites is a method to tailor the rheological and surface properties of the polymer to facilitate better microcell formation and improved mechanical properties.

The batch process of microcellular nanocomposites has been reported (33, 34), where polypropylene/clay nanocomposite and polystyrene/clay nanocomposite specimens were inserted into an autoclave and then saturated with CO_2 under 10 MPa at 135°C and 8.4 MPa at 120°C, respectively. Then, the specimens were allowed to undergo batch foaming when the CO_2 pressure was released. The formed structure was stabilized via cooling to room temperature by water. With the batch process, it was also reported that the exfoliated nanocomposites show a higher viscosity and lead to higher cell density and smaller cell size than the intercalated nanocomposites (34). However, the batch process poses great challenges to industrial production in terms of process economy, throughput, and repeatability. Obviously, the development of continuous or semi-continuous microcellular nanocomposite processes such as injection molding on the industrial scale is more appealing considering the property-to-cost ratio and broader applications. Some research work on microcellular nanocomposite processing has been reported on a continuous extrusion process (35). In this work, the microcellular nanocomposite processing was performed on an industrial 150-ton Toyo injection-molding machine equipped with microcellular injection molding capability (MuCell process). In this study, supercritical N_2, which is more commonly used in microcellular injection molding than CO_2, was used as the physical blowing agent. Investigating the processing benefits and property improvements of combining nanocomposite with the microcellular injection molding process is one of the primary purposes of this research.

EXPERIMENTS

Materials and Experimental Designs

Two batches of PA-6/clay nanocomposites (designated N1 and N2) and their corresponding base PA-6 resins (designated as B1 and B2) were used in this study. These materials are:

Batch 1:
N1 (nanocomposites): RTP-299-A-X-83102-E,
B1 (base resin): RTP-200-A,

Batch 2:
N2 (nanocomposites): RTP-299-A-X-98284-C, and
B2 (base resin): RTP-299-A-X-98284-A

provided by the RTP Company (USA). The base PA-6 resin used in materials N2 and B2 was similar to that used in materials N1 and B1. For the sake of caution and completeness, they are designated differently. Both nanocomposites N1 and N2 contain 5.0% montmorillonite (MMT) clay by weight. These materials were dried for 4 hours at 100°C under vacuum to remove moisture and then injection-molded. The experiments were first executed using materials N1 and B1 based on an L16 orthogonal array fractional factorial design for screening purpose (36). After identifying the important molding parameters, the L9 orthogonal array design (*Table 1*) was then used with materials N2 and B2 in order to enhance the resolution of experiments. As shown in *Table 1*, the L9 experiments contain four different molding parameters (i.e., melt temperature, SCF weight percentage, shot size, and injection speed) at three different levels. For each trial in the L9 experiment, 60 samples were collected. This study was focused on the nanocomposite N2 and its base resin B2. Some additional specific trials were conducted to obtain samples of higher weight reductions and solid samples for the purpose of property comparison.

Testing Techniques

The molded samples (standard dogbone tensile testing bars and straight impact testing bars) were subjected to tensile testing (ASTM-D-638-02) and impact testing (ASTM-D-256-02). The samples were also examined by Scanning Electron Microscopy (JEOL SEM with accelerating voltage of 20 kV), Dynamic Mechanical Analysis (DMA, Rheometrics DMTA-V). SEM and DMA specimens were taken from the middle of the molded dogbone bar. The SEM specimens were characterized both in the melt flow direction and along the

Table 1. L9 Fractional Orthogonal Experimental Design With PA-6/Clay Microcellular Nanocomposite (N2) and Base Resin (B2).

Trial for materials N2 and B2	Melt temperature (C°)		Supercritical content (wt%)		Shot size (mm)		Injection speed (%)	
	Level	Setting	Level	Setting	Level	Setting	Level	Setting
1	1	232	1	0.2	1	16.5	1	20
2	1	232	2	0.4	2	18.4	2	40
3	1	232	3	0.6	3	20.5	3	60
4	2	243	1	0.2	2	18.4	3	60
5	2	243	2	0.4	3	20.5	1	20
6	2	243	3	0.6	1	16.5	2	40
7	3	254	1	0.2	3	20.5	2	40
8	3	254	2	0.4	1	16.5	3	60
9	3	254	3	0.6	2	18.4	1	20

direction normal to the melt flow. Additional SEM micrographs were taken at the tensile testing fracture surfaces. The DMA specimens cut from molding samples were the rectangular strips with dimensions of 40 mm × 4.5 mm × 3.3 mm. The DMA specimen thickness was kept the same as the molding sample to include both the solid layer on part surfaces and the microcellular core of the specimen. This is to avoid inducing residual stresses and damage to the microcellular structure resulting from removing the solid layer. Each specimen was annealed at 85°C for 6 hours before DMA testing to further reduce residual stresses during the molding and cutting processes. Measurements covered temperatures from the room temperature (25°C) up to 220°C at a heating rate of 2°C/min, a frequency of 1 Hz, and 0.1% strain.

Signal-to-Noise Ratio Analyses

To determine the quality characteristics and to optimize the microcellular molding process, the signal-to-noise (S/N) ratio analysis was performed to encapsulate the effect of environmental conditions (outer noise), internal deterioration (inner noise), and variation from unit to unit (between product noise) on those parameters that can be controlled. The relevance of the S/N ratio equation is tied to interpreting the signal or numerator of the ratio as the ability of the process to build good product, or of the product to perform correctly (37). In this specific application of S/N ratio analysis, the tensile strength of molded sample was used in the response calculations. For better tensile strength, the larger-the-better characteristics are looked for. The larger-the-better S/N formulation is expressed as:

$$S/N = -10 \times \log\left(\frac{1/y_1^2 + 1/y_2^2 + \cdots + 1/y_n^2}{n}\right) \quad (1)$$

where y is the experimental measurement of the tensile strength and n is the number of samples per trial. To calculate the S/N ratio, it is commonly accepted to employ the measured data directly as the logarithmic operands without normalization.

An improvement in the molding process or part quality is signified by an increase in the S/N ratio. With the larger-the-better formulation, the S/N increases as the average tensile strength increases. Improved consistency or reduced variability between the measurements also increases the S/N values. The S/N values for tensile strengths for these L9 experiments performed were calculated. By averaging the S/N values for each parameter level, the signal-to-noise response table was generated. By doing so, the effect of a parameter or the rank of a factor can be signified by the difference between the averaged S/N for each level or the difference between the highest and the lowest averaged S/N values. Based on the S/N response table, S/N response graphs were drawn in *Fig. 1*. Instead of plotting averaged mean response (tensile strength) measurements, averaged S/N values were used in *Fig. 1*. The results are discussed in more detail in the following section.

In order to investigate the influence of molding conditions on the cell size and the cell density, the S/N ratio method was also employed. Since it is desirable to have finer microcells, the smaller-the-better S/N formulation was adopted for the cell size analysis and expressed as:

$$S/N = -10 \times \log\left(\frac{y_1^2 + y_2^2 + \cdots y_n^2}{n}\right) \quad (2)$$

where y is the experimental measurement of the cell size, and n is the number of samples per trial. For the cell density study, the larger-the-better S/N formulation in *Eq 1*, where y is the experimental data for the cell density, was still used.

RESULTS AND DISCUSSION

Mechanical Properties

The objective of the design of experiments in this study is to identify the effect of molding parameters on the resulting properties, e.g., tensile strength. With the consideration of control factors and noise factors, the order of precedence of the four molding parameters in these L9 experiments (see *Table 1*) are melt temperature, supercritical fluid percentage by weight, shot size, and injection speed.

From the S/N response table and *Fig. 1*, the molding parameters that affect the tensile strength of microcellular nanocomposite samples N2 are, in order of

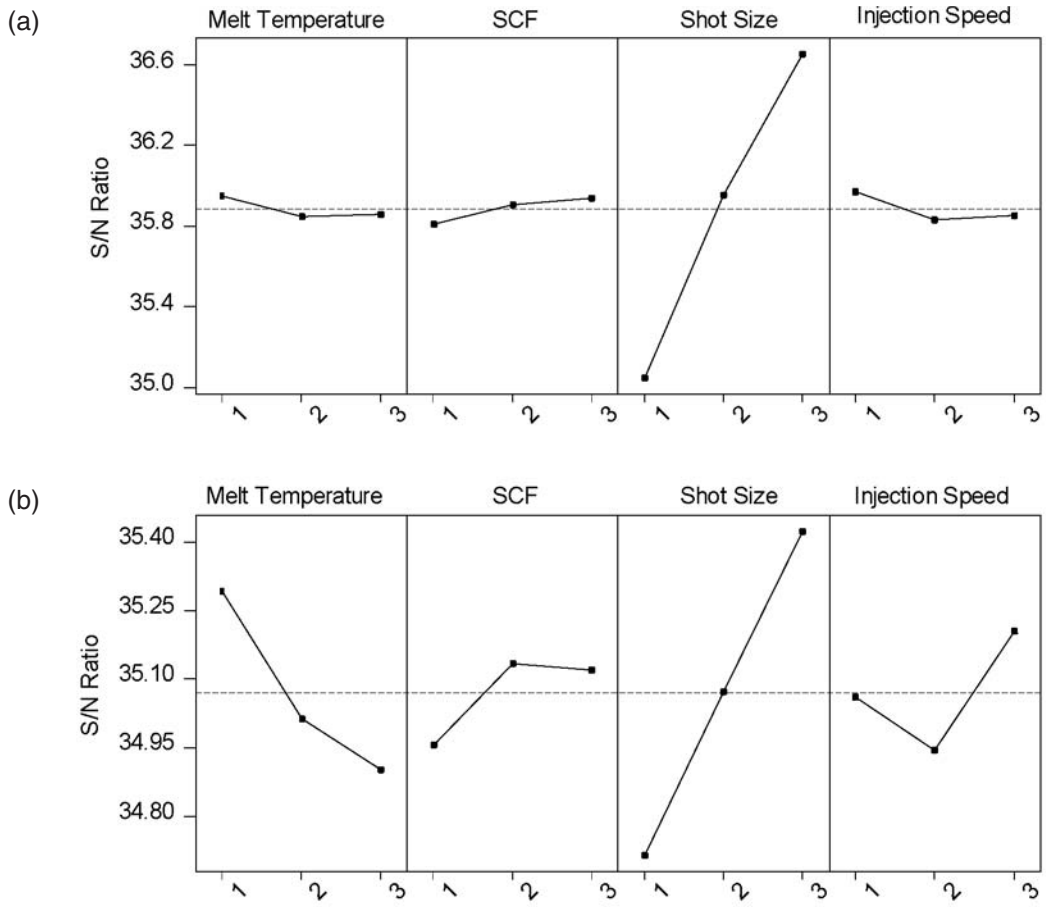

Fig. 1. S/N response for tensile strength with respect to different factors: (a) main effects plot for nanocomposite (N2), (b) main effects plot for base resin (B2).

their influence, shot size, injection speed, supercritical fluid weight percentage, and melt temperature, with the latter three parameters being of much less influence than the first. Based on *Fig. 1*, the recommended optimal molding conditions for the tensile strength are:

1) Shot size: 20.5 mm,
2) Injection speed: 20%,
3) Supercritical fluid weight percentage: 0.6%,
4) Melt temperature: 232°C.

On the other hand, the most important molding parameter for the tensile strength of microcellular base resin samples B2 is shot size, followed by melt temperature, injection speed, and supercritical fluid weight percentage. The recommended levels of these parameters are:

1) Shot size: 20.5 mm,
2) Melt temperature: 232°C,
3) Injection speed: 60%,
4) Supercritical fluid weight percentage: 0.4%.

Apparently, the addition of nano-clay in nanocomposites changes the influence of molding parameters on the tensile properties of the molded parts. Based on this analysis and within the process window selected, a lower melt temperature, higher supercritical fluid weight percentage, higher shot size, and lower injection speed are desirable for better tensile property in microcellular injection molded PA-6/clay parts. It was also observed that the sample weights of microcellular base resin samples B2 fluctuate around their average value at the low melt temperature level but are more consistent at the high melt temperature level. As for the microcellular nanocomposite samples (N2), at all the melt temperature levels, the sample weights are consistent, and the molding process was stable. Overall, the major factor on tensile strength for both microcellular nanocomposites and their microcellular base resin samples is the shot size. Other molding parameters have weaker effects on tensile strength for microcellular base resin samples, and the effects are nearly insignificant for microcellular nanocomposite samples.

The testing results of mechanical property are tabulated in *Table 2*, and some representative stress vs. strain curves are plotted in *Fig. 2*. In *Fig. 2* and the following figures, the suffix following the material symbol represents the trial number of molding condition in *Table 1*. In this work, the measurements were based on the average of eight samples from each trial. As expected, when the same shot size is used or the same

Table 2. Morphological and Mechanical Properties of PA-6/Clay Microcellular Nanocomposite Samples (N2) and PA-6 Microcellular Base Resin Samples (B2).

Trials for materials N2 and B2	Weight reduction*2 (%)		Cell size (microns)		Cell densities (No. of cells/cm^3)		Impact strength (kJ/m^2)		Tensile strength (MPa)	
	N2	B2	N2	B2	N2	B2	N2	B2	N2	B2
0*1	0.0	0.0	—	—	—	—	3.36 ± 0.13	6.36 ± 0.31	83.3 ± 0.7	67.0 ± 0.6
1	18.0	8.8	10.4 ± 7.7	28.7 ± 7.5	1.84E + 08	1.10E + 07	3.47 ± 0.11	5.33 ± 0.28	57.0 ± 0.5	55.0 ± 0.5
2	8.0	7.4	9.1 ± 2.7	53.1 ± 6.7	2.51E + 08	3.27E + 06	2.98 ± 0.05	5.22 ± 0.43	63.0 ± 0.2	57.8 ± 0.2
3	3.4	4.9	55.6 ± 4.6	58.2 ± 18.8	1.58E + 06	1.55E + 06	3.24 ± 0.13	5.09 ± 0.20	68.7 ± 0.2	61.9 ± 0.1
4	8.0	7.4	10.2 ± 3.0	59.6 ± 6.6	1.60E + 08	1.60E + 06	3.26 ± 0.11	4.75 ± 0.28	61.7 ± 0.3	56.5 ± 0.1
5	3.4	5.4	33.7 ± 5.4	38.6 ± 9.6	5.15E + 06	4.74E + 06	2.73 ± 0.09	5.67 ± 0.16	68.6 ± 0.3	59.0 ± 0.1
6	13.1	8.8	13.8 ± 4.0	72.2 ± 27.8	1.19E + 08	6.39E + 05	3.57 ± 0.22	5.15 ± 0.10	56.3 ± 0.6	53.6 ± 0.5
7	8.0	6.4	31.2 ± 6.4	59.3 ± 16.2	6.95E + 06	1.02E + 06	3.47 ± 0.11	5.59 ± 0.11	66.8 ± 0.3	56.3 ± 0.1
8	12.1	8.8	13.8 ± 3.7	33.4 ± 10.6	9.09E + 07	6.91E + 06	3.38 ± 0.05	4.75 ± 0.31	56.3 ± 0.5	54.6 ± 0.3
9	7.3	7.8	10.0 ± 3.1	41.0 ± 18.7	2.26E + 08	2.45E + 06	3.22 ± 0.15	4.84 ± 0.57	63.6 ± 0.5	55.9 ± 0.1

*1 Trial is for the solid sample and the molding is based on the level 2s.
*2 Weight reduction was calculated with sprue and runner.

amount of material is injection molded, the finer and denser microcells in samples usually lead to higher impact strength and less reduction in tensile strength, unless some defects such as coalescence and open cells occur in the cell formation. It was also found that the effect of shot size on mechanical properties is more significant than that of cell size. The stress vs. strain curves of microcellular base resin sample, microcellular nanocomposite sample, and their solid counterparts, are plotted in *Fig. 2a*. Both the solid base resin samples and the solid nanocomposite samples exhibit fairly ductile behavior. The tensile modulus of microcellular nanocomposite sample is higher than that of its corresponding microcellular base resin sample. It should be noted that the ductility and tensile modulus of microcellular nanocomposite depends on the molding conditions, as shown in *Fig. 2b*. The same conclusion can be drawn with the microcellular base resin samples. Compared to solid base resin samples, solid nanocomposite samples have higher tensile strength values but lower Izod impact testing values (cf. *Table 2*). The same behavior is observed with the microcellular nanocomposite and microcellular base resin samples. The ultimate elongation of microcellular sample is smaller than its corresponding solid samples (cf. *Fig. 2a*).

In general, microcellular nanocomposite parts have higher tensile strength but lower impact strength than microcellular base resin parts. The impact of the nanoclays on the mechanical properties, which are also affected by weight reduction, is illustrated in *Fig. 3*. *Figure 3* plots the tensile strength as a function of weight reduction for solid and microcellular nanocomposite samples and the corresponding base resin samples according to *Table 2*. It shows that going from base resin to nanocomposite increases the tensile strength by more than 12% at a constant weight reduction, or equivalently, nanocomposite provides a 9% additional weight reduction for a constant tensile strength, compared to its base resin counterpart.

Morphology

Structure and Distribution of Microcells

With the batch process, it was reported that when the clay concentration of polypropylene (PP)/clay nanocomposite is 2.0 wt%, a closed cell structure with pentagonal and/or hexagonal faces is produced, while the 4.0 wt% and 7.5% wt% clay concentrations result in closed spherical cells (33). However, the network-like closed polygon cell structures are obtained with polystyrene (PS)/clay nanocomposites, even when the clay concentration is as high as 20%. The resulting cell structure is similar to that of foamed base PS, except the cell size is smaller and the cell density is higher (34). In this study, most of the microcells are either closed spherical cells or ellipsoidal cells because of shear flow in the mold cavity, and no obvious polygon and/or network-like cell structures are seen, except that there are some irregular cell structures formed under very high weight-reduction molding conditions. By blending equal amounts of PA-6/clay nanocomposite N2 and its base resin B2, a 2.5 wt% clay concentration was obtained for the microcellular nanocomposite molding process. However, only the spherical cell structures were achieved, as opposed to the pentagonal and/or hexagonal faces of 2.0% PP/clay nanocomposite.

SEM images of microcellular structures and their typical solid boundary layers in this work are shown in *Fig. 4*. Micrographs in *Fig. 4a* through *e* were taken at the centers of the samples. As usual, the micrograph taken at the very center of a sample cross section parallel to the melt flow direction is identical to that perpendicular to the melt flow direction. *Figures 4a* and *4b* present the difference in cell structure between the microcellular nanocomposite, N2, and its base resin, B2, molded under the same molding condition of Trial 3. The nanocomposite has relatively smoother cell walls whereas its base resin has a rougher wall surface. This implies that the nano-clay affects the cell formation and structure directly. *Figures 4a* and *4c*

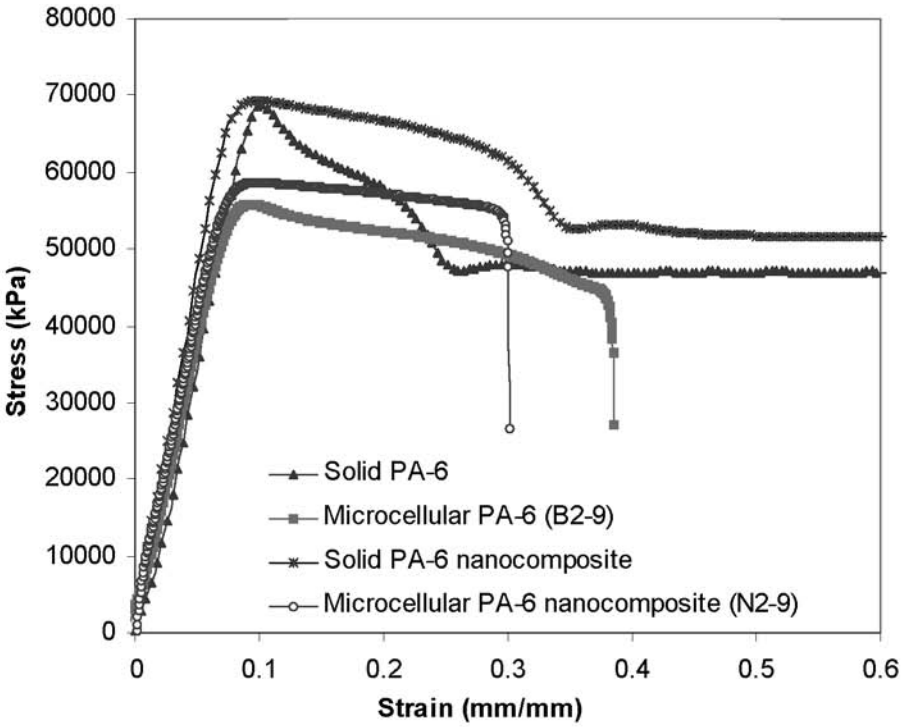

(a)

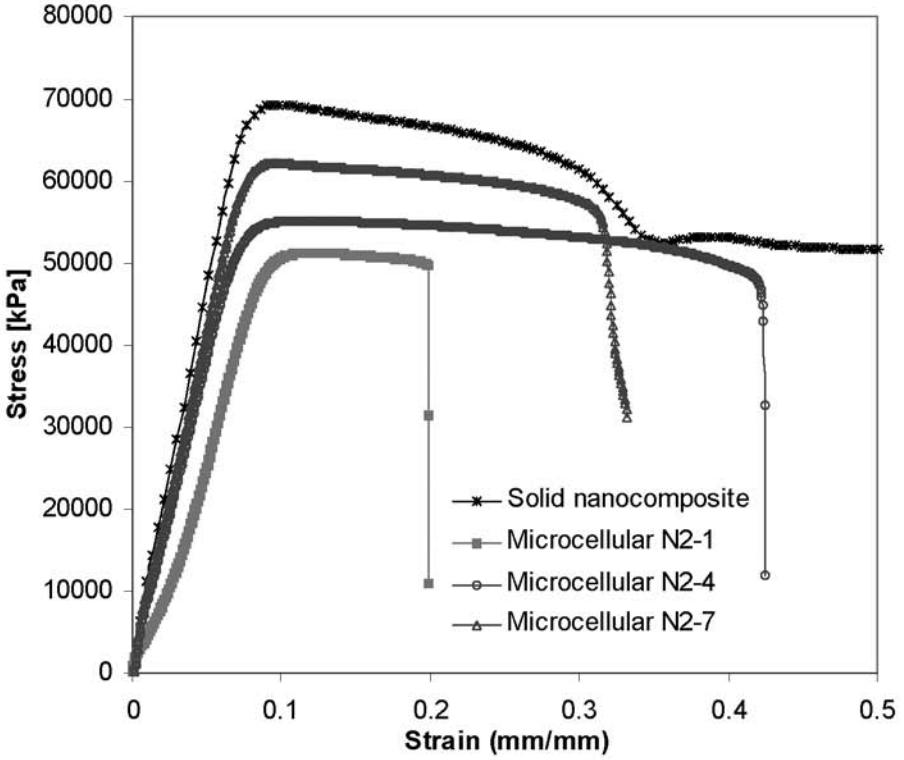

(b)

Fig. 2. Tensile stress vs strain curves of various samples: (a) Comparison of microcellular nanocomposite (N2) and microcellular PA-6 (B2) with their solid counterparts, (b) Comparison of solid and microcellular nanocomposites (N2) under different molding conditions.

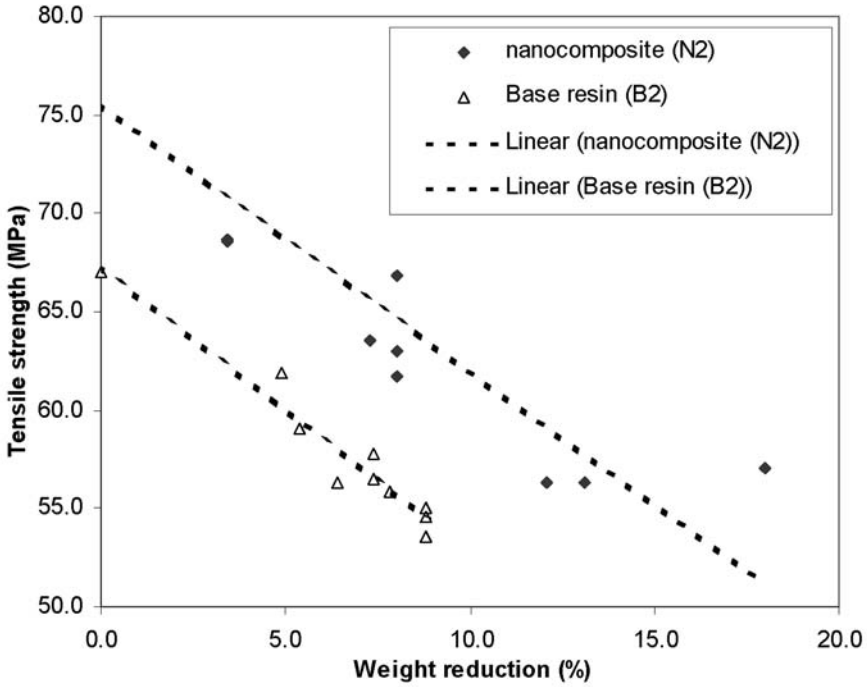

Fig. 3. Correlation of tensile strength and weight reduction for microcellular nanocomposite and base resin samples.

show the comparison of microcellular structures between samples of same nanocomposite under different molding conditions. Even with the same SCF weight percentage, samples of Trial N2-9 in *Fig. 4c* exhibited over 5-fold finer cells than that of Trial N2-3 in *Fig. 4a*. Its cell density is about 150 times higher than that of the latter. Evidently, other molding conditions including shot size, melt temperature, and injection speed also affect the injection pressure and pressure drop rate, all of which collectively influence cell nucleation, cell growth, and thus cell structure. In this case, high melt temperature and small shot size contribute to finer cells.

Figures 4c and *4d* show some controlled nucleation and growth of microcells with the nanocomposite as compared to its base resin under the same molding conditions. Microcells with smoother wall surface observed in the nanocomposite samples were normally smaller than those in the base resin samples, as shown in *Table 2*. In addition, the cell density in the nanocomposite is much higher than that in its base resin. The experiments also show a slightly better control over the cell size at increased gas concentrations, possibly and partially because of a highly dispersed nanoclay phase in the polymer/gas matrix. For the base resin, the microcellular structures under different molding conditions are compared in *Figs. 4b* and *d*. The structural difference between them implies that the molding conditions can greatly affect the cell structure and cell distribution. In *Fig. 4b*, the uniform cell distribution with the molding condition of Trial 3 can be clearly seen. On the other hand, *Fig. 4d* indicates that the molding condition can also improve the cell wall surface quality of the base resin. It seems that at high melt temperature and SCF weight percentage, and low injection speed, the non-uniform cell growth and formation of base resin becomes more obvious, as shown in *Fig. 4d*. The excessive cell growth process can be clearly seen in *Fig. 4e* when the sample weight reduction increases from 7.8% at the B2-9 condition (*Tables 1* and *2*) to 20% by varying the shot size in combination with the SCF weight percentage. This will be further discussed later. It should be mentioned that the sample weight reduction does not solely depend on the shot size because of the inherent shot-volume control variation of the molding machine. In addition, the experimental results in this work show that the weight reduction of sprue and runner follows the same trend as the dogbone part formed in the mold cavity, with the dogbone part weight reduction being slightly higher.

SEM analysis shows that the solid boundary layer of microcellular nanocomposite samples present little structural difference from that of their fully solid counterparts. The micrograph in *Fig. 4f* shows nearly the entire sample cross section normal to the melt flow direction, and the typical and gradual cell structural variation can be seen from the surface layer to the center of sample. For the same sample, along the melt flow direction, elongated microcells are visible in the vicinity of surface layer because of the fountain flow and the shear stress, while uniform spherical cells occur in the center. The deformational pattern of microcells is as shown in *Fig. 7*. These morphological trends were also observed in the microcellular base resin samples.

Similar results were achieved in the microcellular injection molding processes of nanocomposite N1 and its

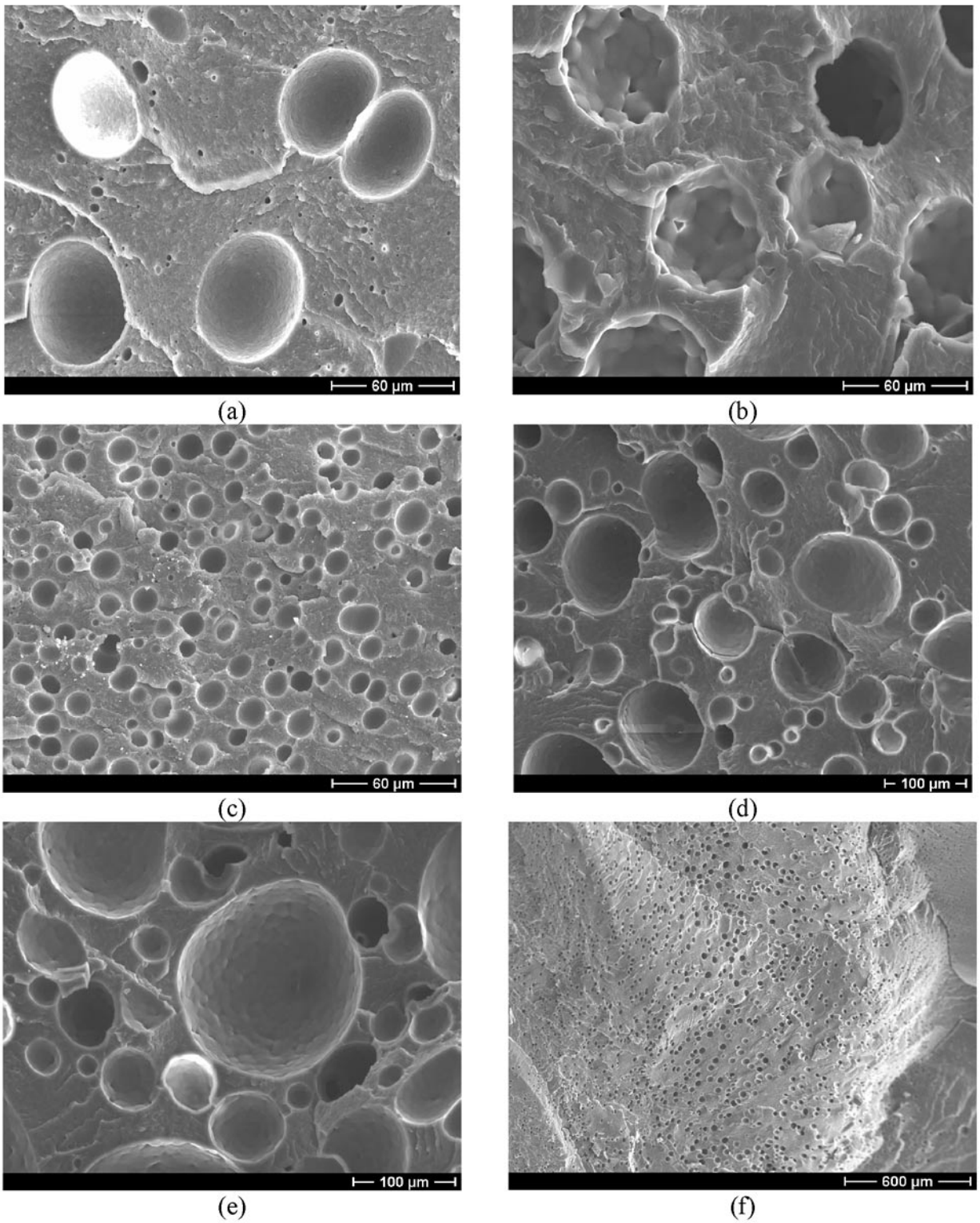

Fig. 4. SEM micrographs of various samples under different molding conditions: (a) along the melt flow direction (N2-3), (b) along the melt flow direction (B2-3), (c) along the melt flow direction (N2-9), (d) along the melt flow direction (B2-9), (e) along the melt flow direction (B2 with weight reduction of 20%), (f) edge and cell structures perpendicular to the melt flow direction (N2-5).

base resin B1. In this work, it is assumed that the crystallization behavior and crystallinity of PA-6 play an important role during the microcell formation. Although much work has been done on the study of crystallization behavior of PA-6/clay nanocomposite (38–40), there has been no report on crystallization behavior of the microcellular nanocomposite. Research on this subject is being undertaken by the authors.

Cell Size and Density

The averaged cell sizes and the cell densities obtained from the SEM analyses for all the L9 DOE trials for nanocomposite N2 and base resin B2 are listed in *Table 2*. From *Table 2*, it can be seen that under the same molding conditions, the microcellular nanocomposite N2 samples have smaller cell sizes and much higher cell densities than the microcellular base resin B2 samples. This phenomenon was also observed for the microcellular nanocomposites N1 and its base resin B1, except for a few special cases. It is believed that the nano-clays may serve as nucleating agents that promote heterogeneous cell nucleation, resulting in higher a cell density. Meanwhile, the increase of viscosity in the nanocomposite hinders the cell growth, leading to a smaller cell size (34).

Through the S/N analyses, the S/N response graphs for the cell densities of nanocomposite N2 and its base resin B2 are shown in *Fig. 5*. From *Fig. 5*, it can be seen that shot size is the only factor that significantly affects the cell density of nanocomposite samples. The maximum cell density was achieved at the medium shot size. It is postulated that a larger shot size leads to higher molding pressure, which hinders cell nucleation, whereas the smaller shot size results in higher cooling rate, and thus lower cell density. More studies would be required in this aspect. Unlike nanocomposites, there is no single molding parameter that predominantly affects the cell density of a base resin. The relative significance of molding factors affecting cell density of base resin in descending order is injection speed > SCF weight percentage > melt temperature > shot size.

The S/N response analysis on the cell size reveals that the shot size is the single molding parameter that significantly affects the cell size of nanocomposites, which is similar to the case for the cell density. The minimum cell size was achieved at the medium shot size. Conceivably, the larger the shot size, the slower the cooling rate, and thus the longer the cooling time promotes more cell growth. On the other hand, with the

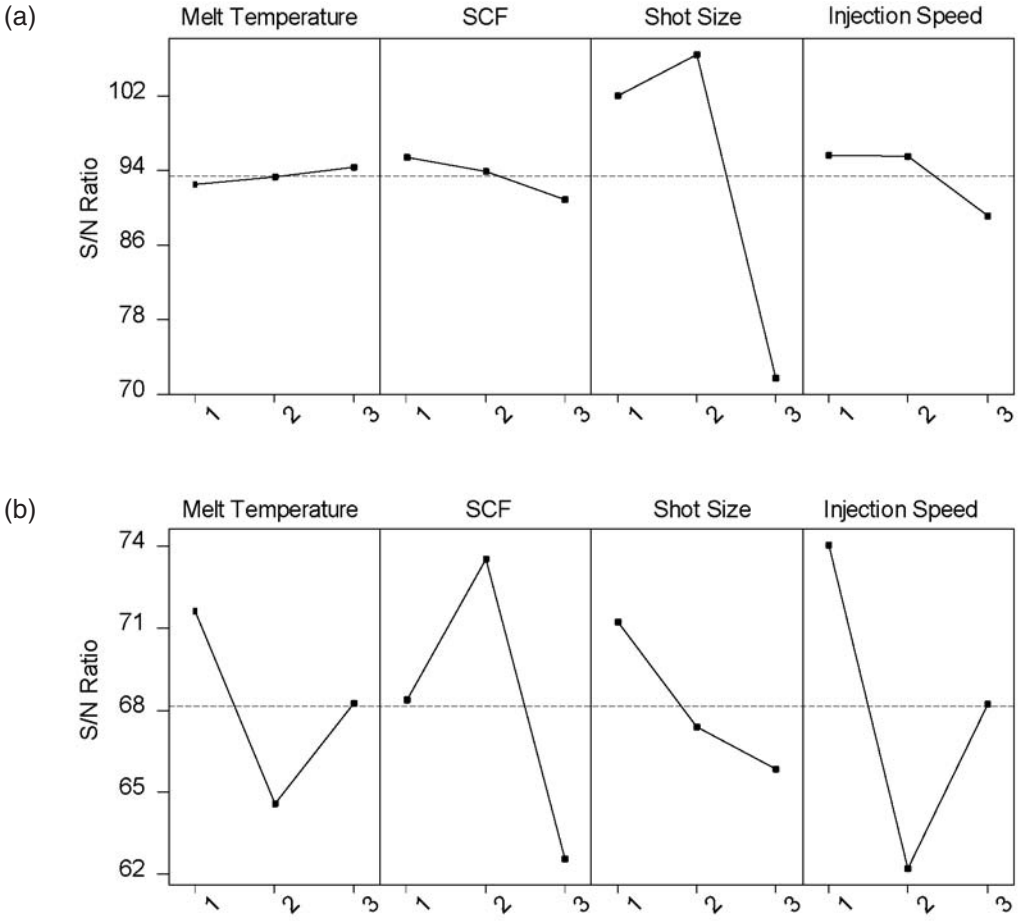

Fig. 5. S/N response for cell density with respect to different factors: (a) main effects plot for nanocomposite (N2), (b) main effects plot for base resin (B2).

smaller shot size, the cells have more space to grow, which is in favor of larger cell sizes. Similar to the case for cell density of base resins, not one single molding factor affects the cell size predominantly. The order of significance of molding parameters is also the same as that for the cell density of base resins.

Morphology Development at High Weight Reductions

As the sample weight reduction increases, the trend of cell growth can be clearly seen (cf. *Figs. 4d* and *4e*). However, the cell structural change can be dramatic when the sample weight reduction exceeds a certain critical value. To obtain the information of cell morphological development, molding trials with higher weight reductions were conducted. The molding parameters used were based on the Trial 9 in the L9 experiments (*Table 1*) with variations of both shot size and SCF content. The evolution of cell structures with increasing weight reductions for the base resin and the nanocomposite are displayed in *Figs. 6* and *7*, respectively. For the base resin, the non-uniform cell growth can be clearly seen, while the cell growth in nanocomposite is relatively uniform. For both the base resin and the nanocomposite, as the weight reduction increases, each cell tends to grow to contact its neighboring ones and a higher degree of cell shear-deformation can be seen. The limit of the uniform cell structure formation is to form the network-like closed cells, in which each cell contacts its neighboring cells without coalescence, as was reported in the batch process (33, 34).

For the nanocomposite at further higher weight reductions, even with the presence of nano-particles in microcellular samples, it was observed that the cell coalescence may take place, and some open cells can also be formed. It is also normal to see irregular cell structures and cell distribution when the sample weight reduction is very high. The big voids can be easily found when the weight reduction of samples exceeds some critical value. These phenomena may be associated with the breakdown of the process window of microcellular injection molding. It is possible that big voids form when the solubility limit of N_2 into the polymer melt is exceeded. It was also observed that cell wall surfaces are still smooth even when irregular cells or big voids form at very high weight reduction conditions.

Fractography

The fractographic structure directly relates to the mechanical properties of the sample. The fractographs of microcellular nanocomposite tensile testing bars are

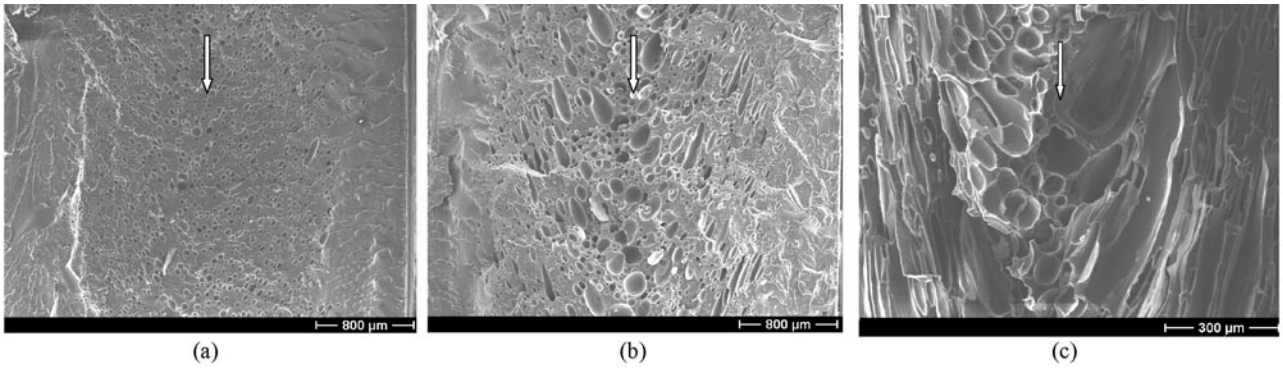

Fig. 6. SEM micrographs of cell structures of microcellular base resin (B2) along the melt flow direction (indicated by arrow): (a) weight reduction 10%, (b) weight reduction 20%, (c) weight reduction 25%.

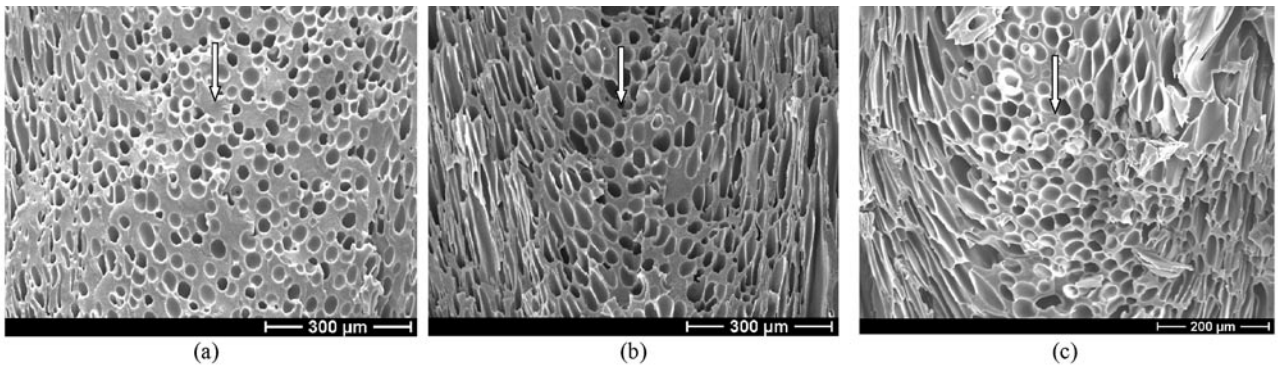

Fig. 7. SEM micrographs of cell structures of microcellular nanocomposite (N1) along the melt flow direction (indicated by arrow): (a) weight reduction 10%, (b) weight reduction 20%, (c) weight reduction 30%.

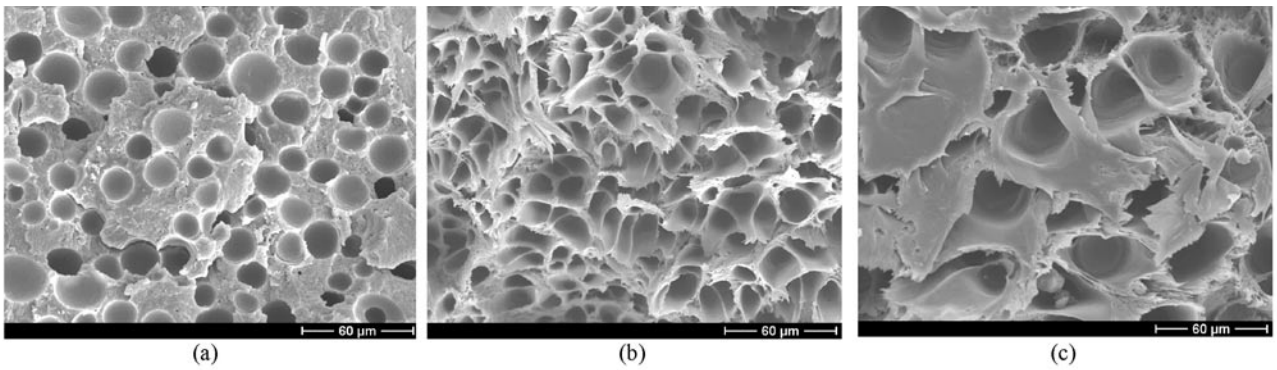

Fig. 8. Fractographs of microcellular nanocomposites: (a) Sample N2-1, (b) Sample N2-4, (c) Sample N2-7.

shown in *Fig. 8* (taken at a quarter length from the edge). Combining with *Fig. 2b*, it can be seen that the molding conditions significantly affect the fracture behavior of microcellular nanocomposites. Based on the textures at the fractured surfaces, the molded samples under different molding conditions can exhibit brittle, ductile, or hybrid fracture behavior. Samples of Trial 1 in *Table 1* (low melt temperature and small shot size) have certain "brittle" fractured structure across the entire cross section (*Fig. 8a*). On the other hand, samples of Trial 7 (high melt temperature and large shot size) show a much more ductile fracture behavior, as demonstrated by the heavily stretched fracture surface throughout the entire cross section (*Fig. 8c*). Samples of Trial 4 (median melt temperature and median shot size), however, exhibit a transition from ductile near the sidewalls to brittle structure in the center.

Four different regions exist at the fractured surfaces of PA-6/clay microcellular nanocomposite tensile bars, as sketched in *Fig. 9*. From the specimen edge to the center, one can find a boundary layer that surrounds the foamed ductile region close to the edge, brittle region near the center, and transitional region in between, respectively. For PA-6/clay nanocomposite, the boundary layer is highly ductile. The transitional region is usually a beltline. Depending on the molding conditions and material properties, only two regions may exist in the single cross section of a sample: boundary layer and brittle region, or boundary layer and ductile region. For the Samples N2-7 shown in *Fig. 8c*, for instance, it was noticed that inside the boundary layer there is only a ductile region. With the decrease or the vanishing of the brittle region, the sample shows more ductile behavior as a whole.

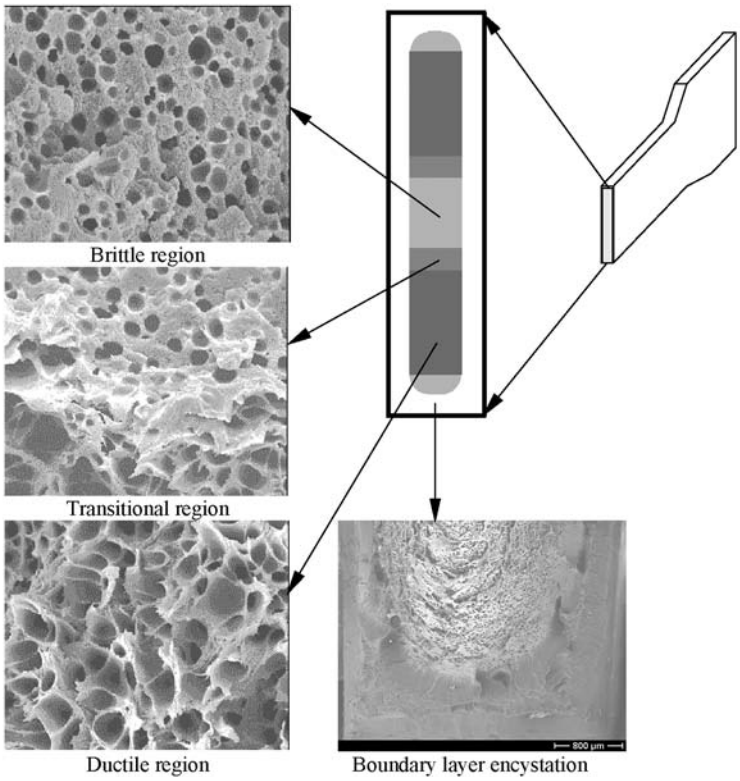

Fig. 9. Schematic of fractured surface on PA-6/clay microcellular nanocomposite part.

Figure 9 also shows that the solid boundary layer has a different fractured structure from the microcellular region. The fractured structure in this solid boundary layer has been found to be the same as that of its fully solid sample. The fractured structure of microcellular region is surrounded by this solid boundary layer, as exemplified in the boundary layer encystation in *Fig. 9*. Compared to the original shape of microcellular region in the sample cross section, after fracture, the shape of microcellular region remains the same, which implies that the microcells play a role in the fracture behavior of the sample.

Dynamic Mechanical Analysis

Many studies have been reported regarding the rheological behavior and morphology of nanocomposites (41–46), but only a few correlate foam structures with rheological properties of nanocomposites (33). For microcellular nanocomposites, dynamic rheological study is of special interest, because the properties of the microcellular nanocomposite depend not only on the bulk properties of the matrix, but also on the size and spacing of the cells as well as the physical and chemical properties of the nano-fillers in the matrix. Some results of studying foams with DMA have been reported (47). But the issues in microcellular nanocomposites are far more complicated because of the additional interfacial phenomena introduced with the clay/polymer/cell structure. In this study, the DMA testing specimens, which contain both of the solid and foamed structures, were cut from the molded samples as described previously. The preliminary results in this study are exemplified in *Fig. 10*. It can be seen that the elastic modulus curves of the microcellular PA-6 sample and the microcellular nanocomposite sample follow the patterns of their corresponding solid counterparts. The elastic modulus of microcellular base resin sample is smaller in magnitude than that of microcellular nanocomposite sample. However, the glass transition temperatures of these molded materials change only slightly. The phase angle curves for the solid and microcellular nanocomposite samples are flatter than those of the solid microcellular base resin samples. These DMA results correlate well with microcellular morphology, where it has been noticed that the cell growth depends strongly on the polymer rheological properties, which are affected greatly by the presence of nano-clays. The increase of viscosity hinders the cell growth and coalescence, resulting in a smaller cell size (34). At the same time, the presence of exfoliated nanoclay platelets may serve as nucleation sites, leading to the high density of microcells.

CONCLUSIONS

Microcellular nanocomposites present a new research area with numerous potential applications. PA-6/clay nanocomposites have been employed in microcellular injection molding to achieve small, uniform microcells with high cell density. Effects of molding conditions on the mechanical properties and microstructure have

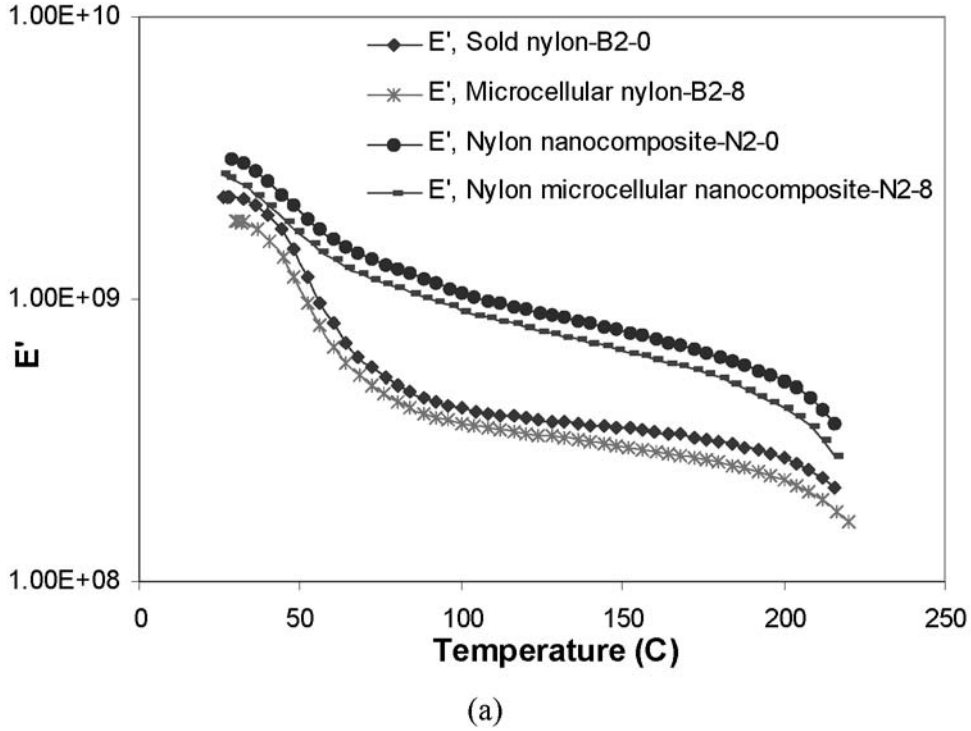

Fig. 10. DMA of microcellular nanocomposite samples (N2-0, N2-8, B2-0, B2-8): (a) elastic modulus change with temperature, (b) phase angle change with temperature.

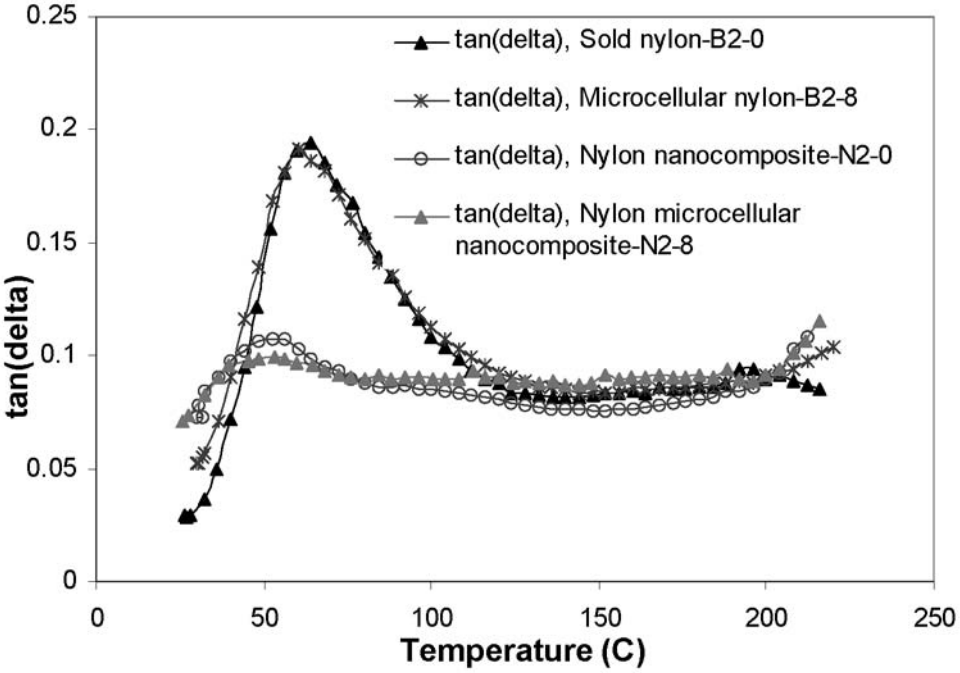

(b)

Fig. 10. Continued.

been studied. Both nano-clay and molding conditions have strong influence on the cell structures and the mechanical properties of the molded samples. The addition of nano-clay promotes the formation of smaller and more uniform cell size and higher cell density. Among the four molding parameters studied, shot size appears to be the most predominant molding parameter affecting the cell size, cell density, and tensile strength in microcellular nanocomposites. On the other hand, the four molding parameters selected seem to have comparable effects on the cell size and cell density in base resins. Microcellular nanocomposites have higher tensile strength but lower impact strength compared to microcellular base resins. Microcellular nanocomposites also exhibit various degrees of ductile behavior. The fractographical study indicates that different regions (boundary layer, ductile, transitional, and brittle) at fractured structures exist that affect the sample's ductility and modes of failure, depending on the molding conditions.

ACKNOWLEDGMENTS

The materials used in the study were generously donated by the RTP Company. Part of this research is supported by the National Science Foundation (DMI-0140396) and the industrial consortium of the Polymer Engineering Center at the University of Wisconsin-Madison. Experimental assistance from Sheila Ruder, Paul Nelson, and Hrishikesh Kharbas is acknowledged.

REFERENCES

1. A. Usuki, Y. Kojima, M. Wkawsumi, A. Okada, Y. Fukushima, T. Kurauchi, and O. Kamigaito, *J. Mater. Res.*, **8(5)**, 1179 (1993).
2. E. P. Giannelis, *Adv. Mater.*, **8(1)**, 29 (1996).
3. R. A. Vaia and E. P. Giannelis, *Macromolecules*, **30(25)**, 8000 (1997).
4. M. Ogawa and K. Kuroda, *Bull. Chem. Soc. Jpn.*, **70**, 2593 (1997).
5. J. W. Gilman, T. Kashiwag, and J. D. Lichtenhan, *SAMPE J.*, **33**, 40 (1997).
6. M. Alexandre and P. Dubois, *Mater. Sci. and Eng. Reports*, **28**, 1 (2000).
7. V. Kumar and J. E. Wells, *SPE ANTEC Tech. Papers*, **38**, 1508 (1992).
8. J. E. Martini, F. A. Waldman, and N. P. Suh, *SPE ANTEC Tech. Papers*, **28**, 674 (1982).
9. D. F. Baldwin and N. P. Suh, *SPE ANTEC Tech. Papers*, **38**, 1503 (1992).
10. K. A. Seeler and V. Kumar, *J. Reinf. Plast.Compos.*, **12**, 359 (1993).
11. M. Shimo, D. F. Baldwin, and N. P. Suh, *SPE ANTEC Tech. Papers*, **39**, 1844 (1993).
12. V. Kumar, *SPE ANTEC Tech. Papers*, **60(2)**, 1892 (2002).
13. S. W. Cha and N. P. Suh, *SPE ANTEC Tech. Papers*, **37**, 1527 (1992).
14. V. Kumar and N. P. Suh, *Polym. Eng. Sci.*, **30**, 1323 (1990).
15. C. B. Park and N. P. Suh, *ASME, Cellular Polymers*, **38**, 69 (1992).
16. S. K. Geol and E. J. Beckman, *Polym. Eng. Sci.*, **34**, 113 (1994).
17. D. F.Baldwin, N. P.Suh, and M. Shimbo, *ASME, Cellular Polymers*, **38**, 109 (1992).
18. C. B. Park and N. P. Suh, *SPE ANTEC Tech Papers*, **39**, 1818 (1993).

19. D. F. Baldwin, N. P. Suh, and M. Shimbo, *ASME, Cellular Polymers,* **38**, 109 (1992).
20. X. Han, K. W. Koelling, D. Tomasko, and L. J. Lee, S*PE ANTEC Tech. Papers,* **46**, 1857 (2000).
21. D. F. Baldwin, C. B. Park, and N. P. Suh, *Polym. Eng. Sci.,* **36**, 1425 (1996).
22. M. Shimbo, K. Nishida, T. Heraku, K. Iijima, T. Sekino, and T. Terayama, *Foams '99, First International Conference on Thermoplastic Foam,* Parsippany, New Jersey, 132 (1999).
23. M. Shimbo, H. Kawashima, and S. Yoshitani, *Foams '2000, Second International Conference on Thermoplastic Foam,* Parsippany, New Jersey, 162 (2000).
24. Kai Jacobsen and David Pierick, *SPE ANTEC Tech. Papers,* **46**, 1929 (2000).
25. J. Xu and D. Pierick, *J. Injection Molding Tech.,* **5**, 152 (2001).
26. V. Kumar and J. E. Weller, *ACS Symposium Series,* **669**, 101 (1997).
27. C. B. Park, *Foam Extrusion,* p. 263, S. Lee, ed., Technomic Publishing Co., Philadelphia (2000).
28. A. I. Cooper, *J. Mater. Chem.,* **10(2)**, 207 (2000).
29. J. Wang, X. Cheng, M. Yuan, and J. He, *Gaofenzi Tongba,* **6**, 8 (2001).
30. W. Michaeli, O. Pfannschmidt, and S. Habibi-Naini, *Kunststoffe,* **92(6)**, 48 (2002).
31. H. Wang, C. Zeng, M. Elkovitch, L. J. Lee, and K. W. Koelling, *Polym. Eng. Sci.,* **41**, 2036 (2001).
32. P. Svoboda, C. Zeng, H. Wang, Y. Yang, H. Li, L. J. Lee, and D. Tomasko, *2002 NSF DMII Grantee and Research Conference,* San Juan, Puerto Rico, (January 2002).
33. P. H. Nam, P. Maiti, M. Okamoto, T. Kotaka, T. Nakayama, M. Takada, M. Ohshima, A. Usuki, N. Hasegawa, and H. Okamoto, *Polym. Eng. Sci.,* **42**, 1907 (2002).
34. C. Zeng, X. Han, L. J. Lee, K. W. Koelling, and D. L. Tomasko, *SPE ANTEC Tech Papers,* **60(2)**, 1504 (2002).
35. X. Han, C. Zeng, L. J. Lee, K. W. Koelling, and D. L. Tomasko, *SPE ANTEC Tech Papers,* **60(2)**, 1915 (2002).
36. H. Kharbas, P. Nelson, M. Yuan, S. Gong, L. Turng, and R. Spindler, *Polym. Compos.,* **24**, 655 (2003).
37. G. S. Peace, *Taguchi Method: A Hands-on Approach,* Addison-Wesley (1993).
38. T. Wu, E. Chen, and C. Liao, *Polym. Eng. Sci.,* **42**, 1141 (2002).
39. M. N. Bureau, J. Denault, K. C. Cole, and G. D. Enright, *Polym. Eng. Sci.,* **42**, 1897 (2002).
40. M. R. Kamal, N. K. Borse, and A. Garcia-Rejon, *Polym. Eng. Sci.,* **42**, 1883 (2002).
41. R. Krishnamoorti and E. P. Giannelis, *Macromolecules,* **30**, 4097 (1997).
42. P. C. LeBaron, Z. Wang, and T. J. Pinnavaia, *Applied Clay Science,* **15**, 11 (1999).
43. M. J. Solomon, A. S. Almusallam, K. F. Seefeldt, and P. Varadan, *219th ACS National Meeting,* San Francisco, (March 2000).
44. J. W. Cho and D. R. Paul, *Polymer,* **42**, 1083 (2001).
45. G. Galgali, C. Ramesh, and A. Lele, *Macromolecules,* **34**, 852 (2001).
46. M. Okamot, P. H. Nam, P. Maiti, and T. Kotaka, *Nanoletter,* **1**, 295 (2001).
47. C. W. Macosko, *NATAS Proceedings,* **18**, 271 (1989).